



Cite this: DOI: 10.1039/c5nj00975h

Highly phosphorescent iridium(III) complexes based on 2-(biphenyl-4-yl)benzo[d]oxazole derivatives: synthesis, structures, properties and DFT calculations†

Zhi-Gang Niu,^{‡a} Tao Zheng,^{‡a} You-Hui Su,^a Peng-Jiang Wang,^a Xiao-Yan Li,^a Feng Cui,^a Jiao Liang^a and Gao-Nan Li^{*ab}

Five new bis-cyclometalated iridium(III) complexes, [(bpbo)₂Ir(acac)] (**3a**), [(fbpbo)₂Ir(acac)] (**3b**), [(Mebpbo)₂Ir(acac)] (**3c**), [(3,5-f₂bpbo)₂Ir(acac)] (**3d**) and [(2,4-f₂bpbo)₂Ir(acac)] (**3e**) (bpbo = 2-(biphenyl-4-yl)benzo[d]oxazole, fbpbo = 2-(4'-fluoro-[biphenyl]-4-yl)benzo[d]oxazole, Mebpbo = (4'-methyl-[biphenyl]-4-yl)benzo[d]oxazole, 3,5-f₂bpbo = 2-(3',5'-difluoro-[biphenyl]-4-yl)benzo[d]oxazole, 2,4-f₂bpbo = 2-(2',4'-difluoro-[biphenyl]-4-yl)benzo[d]oxazole, acac = acetylacetonate), have been synthesized and fully characterized. A single crystal X-ray diffraction study was carried out on complexes **3a–3d**, which showed that each adopted the distorted octahedral coordination geometry with the *cis*-C,C' and *trans*-N,N' arrangement. All Ir(III) complexes are luminescent (560–566 nm) with quantum yields of 3.6–53.5% and lifetimes of 0.282–0.382 μs in solution at 298 K. The spectroscopic and redox characterisation of these complexes were complemented by DFT and TD-DFT calculations, supporting the assignment of ³MLCT/LC to the emissive character.

Received (in Victoria, Australia)
21st April 2015,
Accepted 26th May 2015

DOI: 10.1039/c5nj00975h

www.rsc.org/njc

Introduction

Organic light-emitting diodes (OLEDs), as a promising technology for practical optoelectronic applications, have received considerable attention.^{1–4} Particularly, luminescent iridium-based complexes play an important role in the fabrication of efficient OLEDs on account of their relatively short phosphorescence lifetimes, high quantum efficiencies, easily sublimable feature, and excellent color tenability.⁵

Numerous bis-cyclometalated complexes Ir(C[^]N)₂L, where C[^]N is a cyclometalated ligand and L is a chelating auxiliary ligand, have been synthesized and their spectral properties have been investigated.^{6–9} These studies show that the electro-luminescent efficiency and the emission wavelength of devices are affected mainly by the cyclometalated ligands. To achieve the purpose, one strategy is to change the primary structure of the C[^]N ligand such as pyridine,¹⁰ pyrazine,¹¹ pyridazine,¹² thiazole¹³

and imidazole.¹⁴ Another strategy is to vary the type of substituents on the C[^]N ligand such as electron-withdrawing substituents (–CF₃, –CHO, –CN and –F)¹⁵ and electron-donating substituents (–CH₃, and –OCH₃).¹⁶

In 2001, high-efficiency phosphor [(bo)₂Ir(acac)] (Φ_{em} = 25%) was first reported by Thompson *et al.*¹⁷ Subsequently, [(tbo)₂Ir(acac)], [(tmbo)₂Ir(acac)], [(mpbo)₂Ir(acac)] and [(fmpbo)₂Ir(acac)] were synthesized and used as emitting materials in OLEDs due to their high phosphorescence quantum yield.^{18–21} However, to date, there have been no more reports about (bo)₂Ir(acac) derivatives with substituents on the benzoxazole ring.

To obtain more efficient bo-based Ir(III) complex, the approach we chose was to increase the size of the bo ligand π system and introduce different groups on the C[^]N ligand. Herein, a series of phenyl-modificative benzoxazole cyclometalated ligands (**2a–2e**) has been prepared. Based on these new ligands, five corresponding Ir(III) complexes **3a–3e** have been synthesized. The photophysical and electrochemical properties of these complexes are investigated. Moreover, the absorption spectra are rationalized on the basis of density functional theory (DFT) and time-dependent DFT (TDDFT).

Results and discussion

Synthesis and characterization

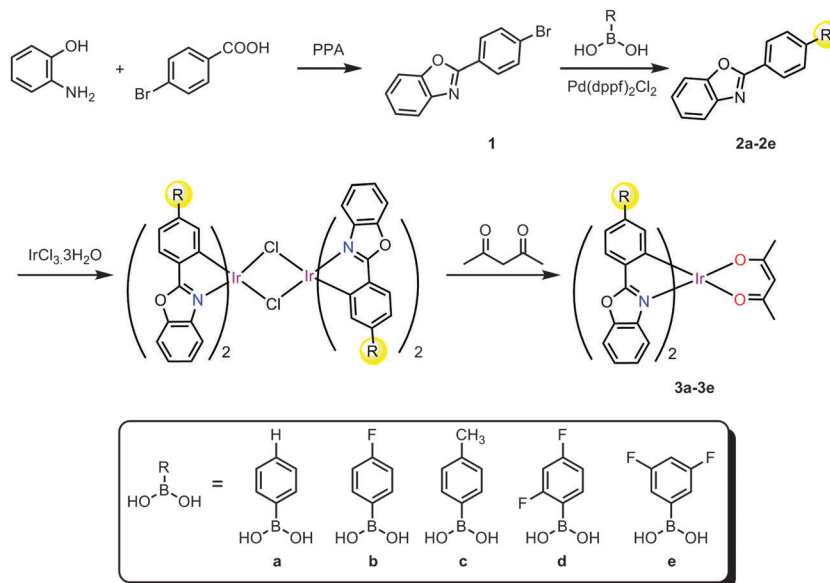
As illustrated in Scheme 1, compound **1** was prepared by the cyclization reaction of 4-bromobenzoic acid with 2-aminophenol

^a College of Chemistry and Chemical Engineering, Hainan Normal University, Haikou 571158, P. R. China. E-mail: ligaonan2008@163.com; Fax: +86-898-6588942; Tel: +86-898-31381637

^b State Key Laboratory of Coordination Chemistry, School of Chemistry and Chemical Engineering, Nanjing University, Nanjing 210093, P. R. China

† Electronic supplementary information (ESI) available: Selected bond distances/angles and additional tables for DFT calculations. CCDC 1055728, 1055767, 1055769 and 1055777. For ESI and crystallographic data in CIF or other electronic format see DOI: 10.1039/c5nj00975h

‡ These authors contributed equally to this work and should be considered co-first authors.

Scheme 1 Synthetic routes of Ir(III) complexes **3a–3e**.

in the presence of polyphosphoric acid (PPA). The cyclometalated ligands **2a–2e** were obtained by the Suzuki reaction between compound **1** and the corresponding substituted phenylboronic acids. Then, the chloride-bridged iridium dimer was synthesized by iridium trichloride hydrate with **2a–2e** according to a similar method reported by Nonoyama.²² Subsequently, the obtained diiridium complexes were converted to iridium(III) complexes **3a–3e** by replacing the two bridging chlorides with a bidentate monoanionic acetylacetonate ligand in good yields.

Structural description

The crystal structures of **3a–3d** were determined by X-ray diffraction analysis, and the ORTEP diagrams are shown in Fig. 1. The crystallographic refinement parameters are listed in Table 1; selected bond lengths and bond angles are shown in Table S1 (ESI[†]).

As shown in Fig. 1, each $[(\text{C}^{\wedge}\text{N})_2\text{Ir}(\text{acac})]$ iridium complex possesses the distorted octahedral coordination geometry with the C and N atoms of bpbo-based cyclometalated ligands and the O atoms of acetylacetonate ancillary ligand. Simultaneously, two bpbo-based ligands adopt *cis*-C,C' and *trans*-N,N' configuration, which is typical for heteroleptic iridium complexes. In all cases, the bond lengths of Ir–N (2.025–2.042 Å), Ir–C (2.002–2.017 Å) and Ir–O (2.123–2.147 Å) are close to those in previously reported $[(\text{C}^{\wedge}\text{N})_2\text{Ir}(\text{acac})]$ systems.^{23,24} The C–Ir–N bite angles of the bpbo-based ligands [79.69(19)–80.58(19)°] are slightly smaller than O–Ir–O bite angles of acac ligands [88.29(9)–89.2(2)°]. This may be due to the rigid effect of the five-membered ring at the metal center.²⁵

In each case, the angles of atoms on the *para* positions of the octahedron range from 174.26(16)° to 176.86(15)° for **3a**, 172.99(18)° to 175.57(17)° for **3b**, 173.92(11)° to 176.36(11)° for **3c** and 172.1(3)° to 176.37(17)° for **3d**. It is noteworthy that two bpbo-based ligands are all pushed away from the ancillary ligands, leading to the fact that N–Ir–N all bend in the reverse direction of acac groups. In addition, one of the phenyl rings is almost fixed in the

parallel position with the benzoxazole ring, whereas another phenyl ring is twisted out of planarity from the aforementioned fragment by 45.948° (**3a**), 38.517° (**3b**), 42.906° (**3c**) and 33.893° (**3d**).

Photophysical properties

The UV-vis absorption spectra of complexes **3a–3e** in CH₂Cl₂ solution are depicted in Fig. 2, and the data are provided in Table 2. All Ir(III) complexes yielded similar absorption spectra. Intense absorption bands from 220 to 360 nm at lower wavelengths are observed, which can be attributed to the spin-allowed ligand-centered $^1\pi\text{-}\pi^*$ transitions arising from both the cyclometalated and ancillary ligands. The mixed spin-allowed $^1\text{MLCT}$ and spin-forbidden $^3\text{MLCT}$ transitions occur in the range of 380–450 nm at longer wavelengths.^{26–29} In comparison with **3a**, the lowest lying absorption bands for complexes **3b–3e** are red-shifted, presumably resulting from substituent changes on the bpbo framework. Moreover, the absorption band in the latter low-energy region is similar, which suggests that the energy gap between HOMO and LUMO are almost the same.

Emission properties

Photoluminescence (PL) emission spectra of complexes **3a–3e** in degassed CH₂Cl₂ solution and in solid state are displayed in Fig. 3, and the corresponding data are also summarized in Table 2. Emission spectra in the solution (Fig. 3a) exhibit the broad emission maxima at 560–566 nm together with a shoulder peak at about 600 nm, indicating that their emissive excited states have $^3\text{MLCT}$ character and ligand-centered (^3LC) character.^{30,31} Specially, the emission bands are significantly red-shifted compared to that of (bo)₂Ir(acac) (525 nm).¹⁷ This is dependent on the fact that the introduction of the phenyl ring into the benzoxazole group expands the conjugation system, which is favourable for the red shift in the emission color.^{17,32,33} As for complex **3d**, an approximately 6 nm red shift relative to the

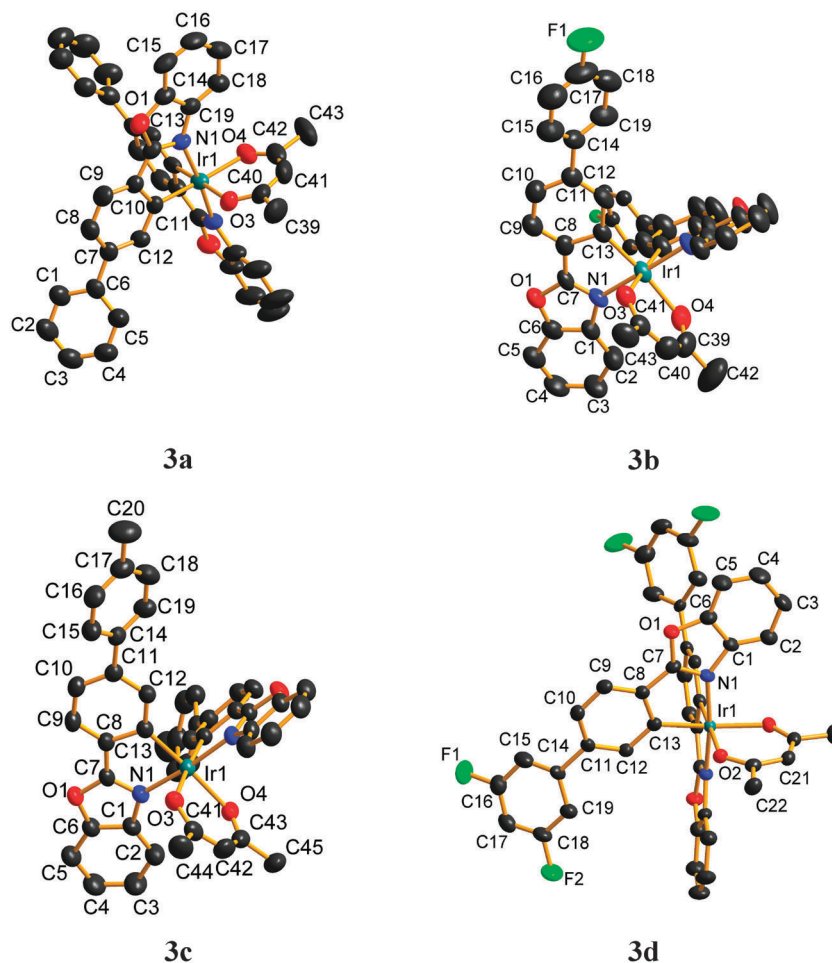


Fig. 1 ORTEP views of **3a–3d** with the atom-numbering scheme at the 50% probability level. Hydrogen atoms and solvent molecules are omitted for clarity.

Table 1 Crystallographic data for complexes **3a–3d**

	3a	3b	3c	2(3d)·CCl₄
Formula	C ₄₃ H ₃₁ IrN ₂ O ₄	C ₄₃ H ₂₉ F ₂ IrN ₂ O ₄	C ₄₅ H ₃₅ IrN ₂ O ₄	C ₈₇ H ₅₄ Cl ₄ F ₈ Ir ₂ N ₄ O ₈
<i>M_r</i>	831.90	867.88	859.97	1961.54
Crystal system	Monoclinic	Monoclinic	Triclinic	Tetragonal
Space group	<i>P</i> ₂ ₁ / <i>n</i>	<i>P</i> ₂ ₁ / <i>n</i>	<i>P</i> $\bar{1}$	<i>P</i> ₄ ₂ / <i>n</i>
Wavelength (Å)	0.7107	0.7107	1.5418	0.7107
X-radiation (graphite monochromator)	Mo-Kα	Mo-Kα	Cu-Kα	Mo-Kα
<i>T</i> (K)	293(2)	293(2)	293(2)	120(10)
<i>a</i> (Å)	10.0973(3)	12.8015(6)	11.2055(3)	14.81340(16)
<i>b</i> (Å)	24.0180(9)	21.5451(8)	12.7447(5)	14.81340(16)
<i>c</i> (Å)	14.6736(4)	13.7718(8)	14.5575(5)	17.0733(4)
α (°)	90	90	65.313(4)	90
β (°)	100.473(3)	112.598(6)	87.690(2)	90
γ (°)	90	90	77.970(3)	90
<i>V</i> (Å ³)	3499.32(19)	3506.7(3)	1844.90(12)	3746.50(11)
<i>Z</i>	4	4	2	2
ρ_c (g cm ⁻³)	1.579	1.644	1.548	1.739
<i>F</i> (000)	1648	1712	856	1924
Absorption coefficient (mm ⁻¹)	3.862	3.865	7.375	3.774
Index ranges	−12 ≤ <i>h</i> ≤ 12 −30 ≤ <i>k</i> ≤ 18 −15 ≤ <i>l</i> ≤ 18	−15 ≤ <i>h</i> ≤ 15 −26 ≤ <i>k</i> ≤ 23 −12 ≤ <i>l</i> ≤ 17	−13 ≤ <i>h</i> ≤ 9 −15 ≤ <i>k</i> ≤ 15 −17 ≤ <i>l</i> ≤ 17	−17 ≤ <i>h</i> ≤ 17 −17 ≤ <i>k</i> ≤ 17 −20 ≤ <i>l</i> ≤ 19
GOF (<i>F</i> ²)	1.065	1.026	1.076	1.054
<i>R</i> ₁ ^a , <i>wR</i> ₂ ^b (<i>I</i> > 2σ(<i>I</i>))	0.0385, 0.0698	0.0480, 0.1051	0.0245, 0.0578	0.0329, 0.0796
<i>R</i> ₁ ^a , <i>wR</i> ₂ ^b (all data)	0.0590, 0.0765	0.0778, 0.1186	0.0290, 0.0605	0.0485, 0.0901

$$^a R_1 = \frac{\sum |F_o| - |F_c|}{\sum |F_o|}, \quad ^b wR_2 = \left[\frac{\sum w(F_o^2 - F_c^2)^2}{\sum w(F_o^2)} \right]^{1/2}.$$

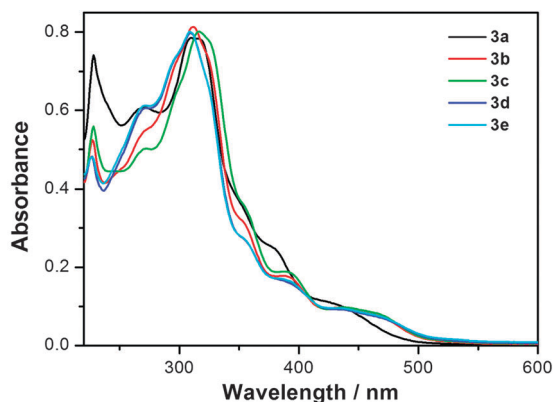


Fig. 2 Absorbance spectra of **3a–3e** in degassed CH_2Cl_2 solution at room temperature.

other four complexes was discovered. The result is dependent on the fluorination on the bpbo ligand. For solid state emissions (Fig. 3b), all these complexes have a stronger bathochromic effect than those in the solution state, which is consistent with the excimer formation arising from π - π stacking interactions in the solid state.²⁸

Phosphorescence relative quantum yields (Φ) of **3a–3e** in dichloromethane solution were measured to be 3.6–53.5% (Table 2) at room temperature using typical phosphorescent *fac*-Ir(ppy)₃ as a standard ($\Phi = 0.40$). Compared with the parent complex **3a** ($\Phi = 0.036$), the introduction of the electron-withdrawing group ($-\text{F}$) in complexes **3b**, **3d** and **3e** result in

the significant increase of the phosphorescence quantum yield. Relatively, the electron-donating group ($-\text{CH}_3$) leads to a weak increase in the phosphorescence quantum yield for complex **3c**. This is probably because the presence of the C-F bonds could reduce the radiationless deactivation rate in comparison with C-H bonds.^{34,35} Remarkably, the emission quantum yield for **3d** is 0.535, which makes it distinctive as the most strongly emissive one in the family of complexes.

Phosphorescence (solution) is observed in all cases with microsecond lifetimes at room temperature, ranging from 0.282 to 0.382 μs , which suggests a possible triplet nature of the emissive excited state. The relatively short “triplet” lifetimes arise from spin-orbit coupling-induced mixing of singlet spin character into the excited state, which, in turn, enhances mixing with the ground state.³⁶

Theoretical calculations

Density functional theory (DFT) and time-dependent DFT (TDDFT) calculations were performed for complexes **3a–3e** to explore the origin of each band in the ultraviolet absorption spectra. The HOMO-LUMO energy-level diagrams for these complexes and the energy gap are presented in Fig. 4. The calculated spin-allowed electronic transitions are provided in Table 3 and Table S2 (ESI[†]), as well as compared with the experimental absorption spectra data. The electron density distributions are summarized in Table S3 (ESI[†]).

We mainly focus on the lowest-energy electronic transition (430 nm for **3a**, 438 nm for **3b**, 438 nm for **3c**, 440 nm for **3d** and

Table 2 Photophysical and electrochemical data for complexes **3a–3e**

Complex	Absorption ^a λ_{abs} (nm)	Emission			Solid λ_{em} /nm
		Solution λ_{em} ^a /nm	τ^a / μs	Φ_{em} ^b /%	
3a	227, 270, 313, 349, 378, 430	562	0.382	3.6	565
3b	225, 270, 312, 353, 390, 438	560	0.282	11.7	560
3c	227, 271, 316, 357, 390, 438	561	0.295	6.0	559
3d	225, 271, 309, 355, 389, 440	566	0.294	31.2	570
3e	226, 271, 309, 355, 388, 438	562	0.313	53.5	560

^a Data were collected from degassed CH_2Cl_2 solutions at room temperature. ^b *fac*-Ir(ppy)₃ as referenced standard (0.4).⁴²

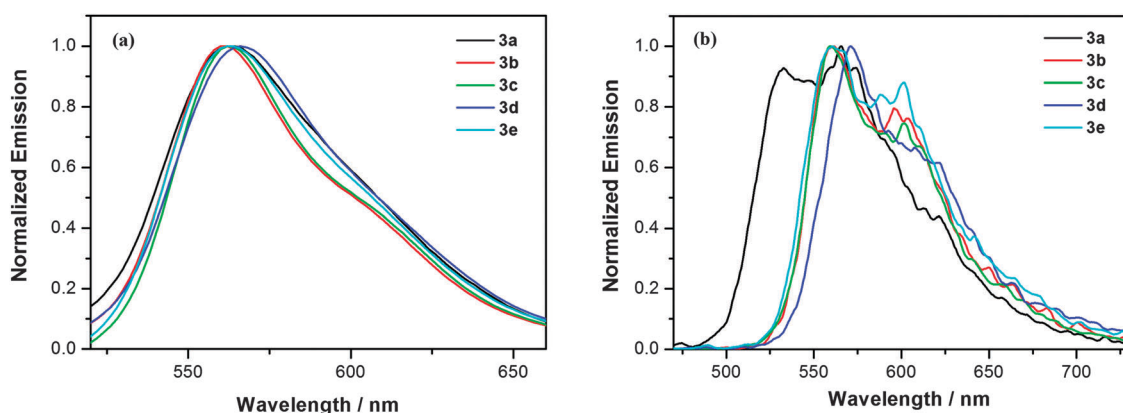


Fig. 3 Normalized emission spectra of **3a–3e** in degassed CH_2Cl_2 solution (a) and solid state (b) at room temperature.

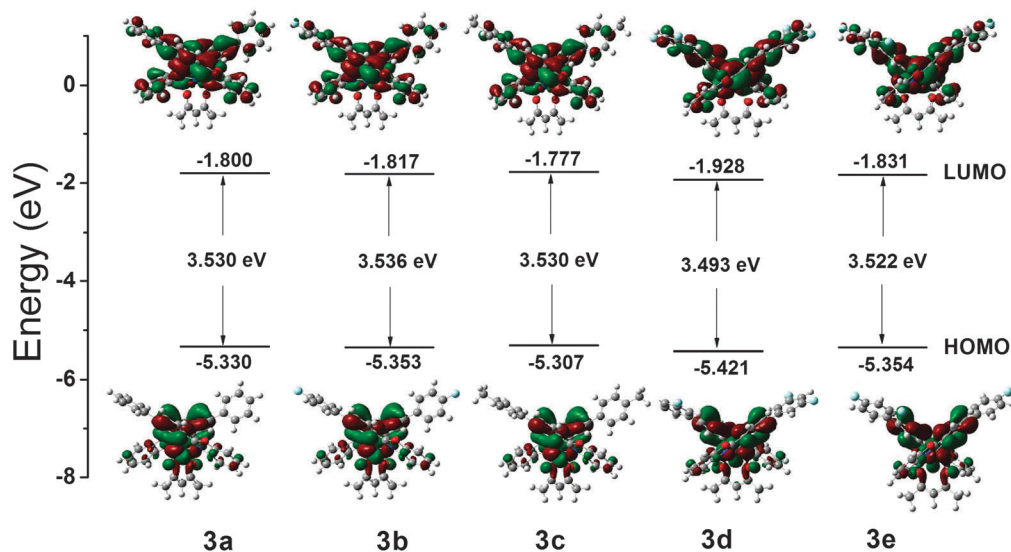


Fig. 4 Molecular orbital energy-level diagrams of HOMOs and LUMOs in the iridium complexes **3a–3e**.

Table 3 Main experimental and calculated optical transitions for complexes **3a–3e**

Complex	Orbital excitations	Nature of transition	Oscillation strength	Calcd (nm)	Exptl (nm)
3a	HOMO → LUMO	Ir(dπ)/L _{bpbo} (π) → L _{bpbo} (π*)	0.1231	439	430
3b	HOMO → LUMO	Ir(dπ)/L _{fbpbo} (π) → L _{fbpbo} (π*)	0.1246	438	438
3c	HOMO → LUMO	Ir(dπ)/L _{Mebpbo} (π) → L _{Mebpbo} (π*)	0.1287	438	438
3d	HOMO → LUMO	Ir(dπ)/L _{3,5-f2bpbo} (π) → L _{3,5-f2bpbo} (π*)	0.1192	443	440
3e	HOMO → LUMO	Ir(dπ)/L _{2,4-f2bpbo} (π) → L _{2,4-f2bpbo} (π*)	0.1171	440	438

438 nm for **3e**). For all species, the electron density in HOMO is mainly dominated by iridium d orbitals and π-orbitals of biphenyl parts of the bpbo ligands, whereas the LUMO is mainly located on the whole bpbo ligands. The TD-DFT-derived optical band gap (HOMO–LUMO) is overestimated for all complexes (Fig. 4 and Table 4), as is expected for such DFT calculations. From Table 3, it can be seen that the HOMO–LUMO transitions of these Ir(III) complexes show a mixed character of the MLCT and the intraligand π–π* transitions. In the cases of **3d**, the fluorination at the 3,5-positions of bpbo moiety lowers the energy levels of HOMO/LUMO and reduces the HOMO–LUMO energy gap, thereby leading to a red-shifted emission. This observation correlates well with the photophysical properties discussed above.

Time-dependent DFT (TDDFT) calculations were performed at the ground state geometries to derive vertical excitation energies

Table 4 Experimental and theoretical HOMO, LUMO, energy band gaps of complexes **3a–3e** (eV)

Complex	E_{ox}	HOMO ^a	$E_{\text{opt,g}}$ ^b	LUMO ^c	HOMO ^d	LUMO ^d
3a	1.18	−5.98	2.39	−3.59	−5.33	−1.80
3b	1.20	−6.00	2.33	−3.67	−5.35	−1.82
3c	1.16	−5.96	2.35	−3.61	−5.31	−1.78
3d	1.26	−6.06	2.30	−3.76	−5.42	−1.93
3e	1.21	−6.01	2.31	−3.70	−5.35	−1.83

^a HOMO energies are deduced from the equation $\text{HOMO} = -(E_{\text{ox}} + 4.8 \text{ eV})$.

^b Optical band gaps obtained from the absorption edge. ^c LUMO = HOMO + $E_{\text{opt,g}}$. ^d Obtained from theoretical calculations.

and hence simulated optical absorption spectra. TDDFT derived spectra for **3a–3e** (with experimental spectra overlaid) are given in Fig. S1 (ESI[†]). From Fig. S1 and Table S2 (ESI[†]), it can be seen that the energies of the calculated transitions are in good agreement with the experimentally recorded spectra.

Electrochemical properties

The electrochemical behaviors of these iridium complexes were investigated by cyclic voltammetry, and the electrochemical waves are shown in Fig. 5. On the basis of these results, the HOMO and LUMO energy levels are also estimated and summarized in Table 4. As depicted in Fig. 5, the complexes **3a–3e** exhibit a reversible one-electron oxidation peak around 1.16–1.26 V, which are attributed to the oxidation of Ir(III) to Ir(IV).^{37,38} On the basis of the potentials of the oxidation, the HOMO energy is deduced by the equation $E_{\text{HOMO}} = -(E_{\text{ox}} + 4.8 \text{ eV})$.³⁹ From the results (Table 4), it can be seen that complexes **3b** and **3e** have the close HOMO values (−6.00 and −6.01 eV), which are lower than that of **3a** (−5.98 eV), and **3d** has the lowest one of all (−6.06 eV). On the contrary, **3c** has the highest HOMO values (−5.96 eV). These findings indicate that the electron-donating group (−CH₃) can improve the HOMO energy levels, whereas the electron-withdrawing fluorine atoms lower them effectively, particularly the substitution of F at the 3,5-position. As compared with the theoretical calculation results, it can be seen that the HOMO orbital energy also reveals the order as **3c** > **3a** > **3b** ≈ **3e** > **3d**. The energy levels of the lowest unoccupied molecular orbital (LUMO) were obtained from the HOMO and $E_{\text{opt,g}}$ values.

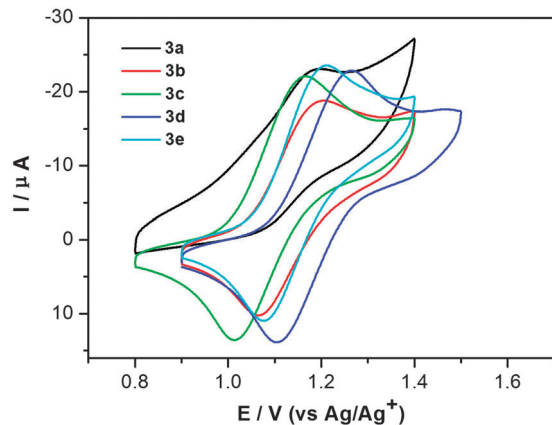


Fig. 5 Cyclic voltammograms for complexes **3a–3e** in CH_2Cl_2 solution containing $n\text{-Bu}_4\text{NClO}_4$ (0.1 M) at a sweep rate of 100 mV s^{-1} .

It can be observed that **3d** has the lowest LUMO energy level compared with other complexes based on experimental and theoretical data, indicating the stabilization of the LUMO orbital. In addition, the $E_{\text{opt,g}}$ values obtained from the absorption edge have similar values ranging from 2.30 to 2.39 eV. The variation tendency of band gaps obtained from experimental characterization is approximately consistent with those obtained from DFT calculations (Fig. 4).

Conclusion

In summary, a new family of cyclometalated $[(\text{C}^{\wedge}\text{N})_2\text{Ir}(\text{acac})]$ iridium(III) complexes **3a–3e** with two bpbo-based main ligands and one acac ancillary ligand, has been synthesized and characterized. Their photophysical properties, theoretical calculations and electrochemical behaviors have been investigated. The molecular structures of complexes **3a–3d** reveal that they all possess pseudo-octahedral coordination geometry. Each Ir(III) complex exhibits a yellow emission with a maximum main peak and a shoulder peak, which is suggested to be a mixture of ${}^3\text{LC}$ (${}^3\pi\text{-}\pi^*$) and ${}^3\text{CT}$ (${}^3\text{MLCT}$) excited states. The theoretical calculations have also been performed to rationalize the photophysical and electrochemical properties.

Experimental section

General methods

${}^1\text{H}$ NMR spectra were recorded using a Bruker AM 400 MHz instrument. Chemical shifts were reported in ppm relative to Me_4Si as internal standard. ESI-MS and MALDI-TOF-MS spectra were recorded using an Esquire HCT-Agilent 1200 LC/MS spectrometer and a Bruker Autoflex IITM TOF/TOF instrument, respectively. UV-vis spectra were recorded using a Hitachi U3900/3900H spectrophotometer. Fluorescence spectra were carried out using a Hitachi F-7000 spectrophotometer. Luminescence lifetime curves were measured using an Edinburgh Instruments FLS920P fluorescence spectrometer, and the data were treated as one-order exponential fitting using OriginPro 8 software.

The luminescence quantum efficiencies were calculated by comparison of the fluorescence intensities (integrated areas) of a standard sample $\text{fac-Ir}(\text{ppy})_3$ and the unknown sample according to the equation^{40–42}

$$\Phi_{\text{unk}} = \Phi_{\text{std}} \left(\frac{I_{\text{unk}}}{I_{\text{std}}} \right) \left(\frac{A_{\text{std}}}{A_{\text{unk}}} \right) \left(\frac{\eta_{\text{unk}}}{\eta_{\text{std}}} \right)^2$$

where Φ_{unk} and Φ_{std} are the luminescence quantum yield values of the unknown sample and $\text{fac-Ir}(\text{ppy})_3$ solutions ($\Phi_{\text{std}} = 0.4$),⁴² respectively. I_{unk} and I_{std} are the integrated fluorescence intensities of the unknown sample and $\text{fac-Ir}(\text{ppy})_3$ solutions, respectively. A_{unk} and A_{std} are the absorbance values of the unknown sample and $\text{fac-Ir}(\text{ppy})_3$ solutions at their excitation wavelengths, respectively. η_{unk} and η_{std} represent the refractive indices of the corresponding solvents (pure solvents were assumed).

Materials

$\text{IrCl}_3 \cdot 3\text{H}_2\text{O}$ and other chemicals were obtained from commercial resources and used without further purification. All solvents were purified and dried by standard procedures. All of the reactions dealing with air sensitive reactions were carried out in a nitrogen atmosphere.

Syntheses

2-(4-Bromophenyl)benzo[d]oxazole (1). A mixture of 2-hydroxybenzoic acid (920 mg, 4.58 mmol) and 2-aminophenol (500 mg, 4.58 mmol) in polyphosphoric acid (20 mL) was heated at 180°C under nitrogen for 2 h. The reaction mixture was poured into ice-water and adjusted to pH = 8–9 by addition of solid NaOH. The mixture was extracted with ethyl acetate, and the combined organic layers were washed with brine. After drying with anhydrous Na_2SO_4 , the crude product was purified by column chromatography with petroleum ether/ethyl acetate (100:1) to afford pure product **1** (765 mg, yield: 60.9%) as a white solid. ${}^1\text{H}$ NMR (400 MHz, CDCl_3) δ 8.14 (d, $J = 7.6$ Hz, 2H), 7.77–7.79 (m, 1H), 7.68 (d, $J = 8.0$ Hz, 2H), 7.59–7.60 (m, 1H), 7.37–7.39 (m, 2H). MS-ESI: m/z 274.1, 276.1 ($M + 1$).

2-([Biphenyl]-4-yl)benzo[d]oxazole (bpbo, 2a). A mixture of **1** (150 mg, 0.55 mmol), benzenboronic acid (80 mg, 0.66 mmol), $\text{Pd}(\text{dppf})_2\text{Cl}_2$ (25 mg) and potassium acetate (230 mg, 1.66 mmol) was dissolved in anhydrous 1,4-dioxane (10 mL) and heated at 90°C under nitrogen for 10 h. After cooling to room temperature, the mixture was poured into water (20 mL) and extracted with dichloromethane. The combined organic layers were dried with anhydrous Na_2SO_4 and concentrated in vacuum. The crude product was purified by column chromatography with petroleum ether/ethyl acetate (50:1) eluent to afford pure product **2a** (135 mg, yield: 90.9%) as a white solid. ${}^1\text{H}$ NMR (400 MHz, CDCl_3) δ 8.35 (d, $J = 8.0$ Hz, 2H), 7.77–7.79 (m, 3H), 7.69 (d, $J = 7.2$ Hz, 2H), 7.59–7.61 (m, 1H), 7.48 (d, $J = 7.2$ Hz, 2H), 7.39–7.43 (m, 3H). MS-ESI: m/z 272.2 ($M + 1$).

2-(4'-Fluoro-[biphenyl]-4-yl)benzo[d]oxazole (fbpbo, 2b). **2b** was obtained by a method similar to the preparation of **2a** using 4-fluorophenylboronic acid instead of benzenboronic acid (152 mg, yield: 92.4%). ${}^1\text{H}$ NMR (400 MHz, CDCl_3) δ 8.34

(d, $J = 8.0$ Hz, 2H), 7.79–7.81 (m, 1H), 7.72 (d, $J = 8.0$ Hz, 2H), 7.61–7.66 (m, 3H), 7.37 (dd, $J_1 = 2.4$ Hz, $J = 8.8$ Hz, 2H), 7.17 (d, $J = 8.4$ Hz, 2H). MS-ESI: m/z 290.1 (M + 1).

(4'-Methyl-[biphenyl]-4-yl)benzo[d]oxazole (Mebpbo, 2c). 2c was obtained by a method similar to the preparation of 2a using 4-methylphenylboronic acid instead of benzenboronic acid (161 mg, yield: 91.7%). $^1\text{H NMR}$ (400 MHz, CDCl_3) δ 8.32 (d, $J = 8.0$ Hz, 2H), 7.75–7.80 (m, 3H), 7.57–7.62 (m, 3H), 7.37–7.38 (m, 2H), 7.30 (d, $J = 7.6$ Hz, 2H), 2.43 (s, 3H). MS-ESI: m/z 286.1 (M + 1).

2-(3',5'-Difluoro-[biphenyl]-4-yl)benzo[d]oxazole (3,5-f₂bpbo, 2d). 2d was obtained by a method similar to the preparation of 2a using 3,5-difluorophenylboronic acid instead of benzenboronic acid (168 mg, yield: 91.6%). $^1\text{H NMR}$ (400 MHz, CDCl_3) δ 8.34 (d, $J = 7.6$ Hz, 2H), 7.80 (dd, $J_1 = 3.2$ Hz, $J_2 = 6.0$ Hz, 1H), 7.71 (d, $J = 8.4$ Hz, 2H), 7.61 (dd, $J_1 = 3.2$ Hz, $J_2 = 6.0$ Hz, 1H) 7.36–7.41 (m, 2H), 7.18 (d, $J = 6.8$ Hz, 2H), 6.82–6.88 (m, 1H). MS-ESI: m/z 308.2 (M + 1).

2-(2',4'-Difluoro-[biphenyl]-4-yl)benzo[d]oxazole (2,4-f₂bpbo, 2e). 2e was obtained by a method similar to the preparation of 2a using 2,4-difluorophenylboronic acid instead of benzenboronic acid (153 mg, yield: 90.3%). $^1\text{H NMR}$ (400 MHz, CDCl_3) δ 8.34 (d, $J = 8.0$ Hz, 2H), 7.79–7.82 (m, 1H), 7.69 (d, $J = 8.0$ Hz, 2H), 7.60–7.63 (m, 1H), 7.45–7.51 (m, 1H), 7.37–7.40 (m, 2H), 6.93–7.02 (m, 2H). MS-ESI: m/z 308.2 (M + 1).

(bpbo)₂Ir(acac) (3a). A mixture of $\text{IrCl}_3 \cdot 3\text{H}_2\text{O}$ (40 mg, 0.13 mmol) and the ligand 2a (76 mg, 0.28 mmol) in 6 mL of ethoxyethanol and H_2O ($v:v = 2:1$) was refluxed for 12 h. Upon cooling to room temperature, the orange precipitate was collected by filtration and washed with cooled ether and MeOH. After drying, the crude product of chloro-bridged iridium dimer was used directly in the next step without further purification. A mixture of the abovementioned dimer, pentane-2,4-dione (5.0 equiv.) and Na_2CO_3 (8.0 equiv.) was dissolved in ethoxyethanol (5 mL) and refluxed for 10 h under nitrogen. The mixture was poured into water, and the precipitate was collected. The crude solid was purified by column chromatography with petroleum ether/dichloromethane (10:1) eluent to afford pure product 3a (29 mg, yield: 56.9%) as an orange solid. $^1\text{H NMR}$ (400 MHz, CDCl_3) δ 7.70–7.74 (m, 7H), 7.40–7.46 (m, 5H), 7.13–7.26 (m, 10H), 6.72 (s, 2H), 5.30 (s, 1H), 1.89 (s, 6H). MS (MALDI-TOF): $m/z = 834.52, 735.09$ (M-acac).

(fbpbo)₂Ir(acac) (3b). 3b was obtained by a method similar to the preparation of 3a as an orange solid (23 mg, yield: 58.7%). $^1\text{H NMR}$ (400 MHz, CDCl_3) δ 7.70–7.74 (m, 4H), 7.60 (d, $J = 7.6$ Hz, 2H), 7.42–7.50 (m, 4H), 7.16–7.29 (m, 4H), 7.06 (d, $J = 8.0$ Hz, 2H), 6.90–6.94 (m, 4H), 6.65 (s, 2H), 5.29 (s, 1H), 1.89 (s, 6H). MS (MALDI-TOF): $m/z = 870.55, 771.14$ (M-acac).

(Mebpbo)₂Ir(acac) (3c). 3c was obtained by a method similar to the preparation of 3a as an orange solid (22 mg, yield: 53.6%). $^1\text{H NMR}$ (400 MHz, CDCl_3) δ 7.68–7.72 (m, 4H), 7.61 (d, $J = 6.8$ Hz, 2H), 7.41–7.48 (m, 4H), 7.09–7.26 (m, 8H), 7.05 (d, $J = 7.6$ Hz, 2H), 6.71 (s, 2H), 5.29 (s, 1H), 2.29 (s, 6H), 1.89 (s, 6H). MS (MALDI-TOF): $m/z = 862.62, 763.18$ (M-acac).

(3,5-f₂bpbo)₂Ir(acac) (3d). 3d was obtained by a method similar to the preparation of 3a as an orange solid (21 mg, yield: 57.7%). $^1\text{H NMR}$ (400 MHz, CDCl_3) δ 7.74 (t, $J = 7.2$ Hz, 4H), 7.61

(d, $J = 7.2$ Hz, 2H), 7.44–7.53 (m, 4H), 7.07 (d, $J = 7.6$ Hz, 2H), 6.71 (d, $J = 7.6$ Hz, 4H), 6.60–6.65 (m, 4H), 5.30 (s, 1H), 1.89 (s, 6H). MS (MALDI-TOF): $m/z = 906.56, 807.14$ (M-acac).

(2,4-f₂bpbo)₂Ir(acac) (3e). 3e was obtained by a method similar to the preparation of 3a as an orange solid (23 mg, yield: 54.2%). $^1\text{H NMR}$ (400 MHz, CDCl_3) δ 7.68–7.73 (m, 4H), 7.59 (d, $J = 6.8$ Hz, 2H), 7.42–7.47 (m, 4H), 7.03–7.09 (m, 4H), 6.69–6.74 (m, 4H), 6.60 (s, 2H), 5.28 (s, 1H), 1.82 (s, 6H). MS (MALDI-TOF): $m/z = 906.55, 807.13$ (M-acac).

X-ray structure determination

X-ray diffraction data were collected with an Agilent Technologies Gemini A Ultra diffractometer equipped with graphite-monochromated Mo $K\alpha$ radiation ($\lambda = 0.7107 \text{ \AA}$) and Cu $K\alpha$ radiation ($\lambda = 1.5418 \text{ \AA}$) at room temperature. Data collection and reduction were processed with CrysAlisPro software.⁴³ All of the structures were solved using Superflip⁴⁴ and refined using SHELXL-2014⁴⁵ within Olex2.⁴⁶ All non-hydrogen atoms were found in alternating difference Fourier syntheses and least-squares refinement cycles, and during the final cycles, refined anisotropically. Hydrogen atoms were placed in calculated positions and refined as riding atoms with a uniform value of U_{iso} .

Electrochemical measurements

Cyclic voltammetry (CV) was performed using a CHI 1210B electrochemical workstation, with a glassy carbon electrode as the working electrode, a platinum wire as the counter electrode, an Ag/Ag^+ electrode as the reference electrode, and 0.1 M $n\text{-Bu}_4\text{NClO}_4$ as the supporting electrolyte.

Computational details

All calculations were carried out with the Gaussian 09 software package.⁴⁷ The density functional theory (DFT) and time-dependent DFT (TDDFT) were employed with no symmetry constraints to investigate the optimized geometries and electron configurations with the Becke three-parameter Lee–Yang–Parr (B3LYP) hybrid density functional theory.^{48–50} The LANL2DZ basis set was used to treat the Ir atom, whereas the 6-31G* basis set was used to treat C, H, O, N and F atoms. Solvent effects were considered within the SCRF (self-consistent reaction field) theory using the polarized continuum model (PCM) approach to model the interaction with the solvent.^{51,52}

Acknowledgements

This work was supported by the Natural Science Foundation of Hainan Province (No. 20152017), the Science and Research Project of Education Department of Hainan Province (Nos. Hjkj2013-25 and Hnky2015-27) and Hainan Provincial Innovation Experiment Program for University Students (No. 20140053).

Notes and references

- M. A. Baldo, M. E. Thompson and S. R. Förrest, *Pure Appl. Chem.*, 1999, **71**, 2095.

- 2 C. Adachi, M. A. Baldo, D. F. O'Brien, M. E. Thompson and S. R. Forrest, *J. Appl. Phys.*, 2001, **90**, 5048.
- 3 M. Ikai, S. Tokito, Y. Sakamoto, T. Suzuki and Y. Taga, *Appl. Phys. Lett.*, 2001, **79**, 156.
- 4 S.-C. Lo, N. A. H. Male, J. P. J. Markham, S. W. Magennis, P. L. Burn, O. V. Salata and I. D. W. Samuel, *Adv. Mater.*, 2002, **14**, 975.
- 5 M. A. Baldo, M. E. Thompson and S. R. Forrest, *Nature*, 2000, **403**, 750.
- 6 P. J. Hay, *J. Phys. Chem. A*, 2002, **106**, 1634.
- 7 A. B. Tamayo, B. D. Alleyne, P. I. Djurovich, S. Lamansky, I. Tsyba, N. N. Ho, R. Bau and M. E. Thompson, *J. Am. Chem. Soc.*, 2003, **125**, 7377.
- 8 J. P. Collin, I. M. Dixon, J. P. Sauvage, J. A. G. Williams, F. Barigelletti and L. Flamigni, *J. Am. Chem. Soc.*, 1999, **121**, 5009.
- 9 I. M. Dixon, J. P. Collin, J. P. Sauvage and L. Flamigni, *Inorg. Chem.*, 2001, **40**, 5507.
- 10 Z. Liu, I. R. Canelon, A. Habtemariam, G. J. Clarkson and P. J. Sadler, *Organometallics*, 2014, **33**, 5324.
- 11 K. Hasan, L. Donato, Y. L. Shen, J. D. Slinker and E. Z. Colman, *Dalton Trans.*, 2014, **43**, 13672.
- 12 Y. Fang, Y. H. Li, S. J. Wang, Y. Z. Meng, J. B. Peng and B. Wang, *Synth. Met.*, 2010, **160**, 2231.
- 13 T. Giridhar, W. Cho, Y.-H. Kim, T.-H. Han, T.-W. Lee and S.-H. Jin, *J. Mater. Chem. C*, 2014, **2**, 9398.
- 14 K. P. Klubek, S. C. Dong, L. S. Liao, C. W. Tang and L. J. Rothberg, *Org. Electron.*, 2014, **15**, 3127.
- 15 Z. G. Niu, D. Liu, J. Zuo, Y. Zou, J. M. Yang, Y. H. Su, Y. D. Yang and G. N. Li, *Inorg. Chem. Commun.*, 2014, **43**, 146.
- 16 I. R. Laskar and T. M. Chen, *Chem. Mater.*, 2004, **16**, 111.
- 17 S. Lamansky, P. Djurovich, D. Murphy, F. Abdel-Razzaq, H. E. Lee, C. Adachi, P. E. Burrows, S. R. Forrest and M. E. Thompson, *J. Am. Chem. Soc.*, 2001, **123**, 4304.
- 18 L. Chen, C. Yang, J. Qin, J. Gao and D. Ma, *Inorg. Chim. Acta*, 2006, **359**, 4207.
- 19 X. Li, X. T. Yu, H. J. Chi, Y. Dong, G. Y. Xiao, P. Lei, D. Y. Zhang and Z. Cui, *Spectrochim. Acta, Part A*, 2013, **116**, 473.
- 20 X. Li, H. J. Chi, Y. Dong, G. Y. Xiao, P. Lei, D. Y. Zhang and Z. Cui, *Opt. Mater.*, 2013, **36**, 265.
- 21 H. W. Hong and T. M. Chen, *Mater. Chem. Phys.*, 2007, **101**, 170.
- 22 M. Nonoyama, *Bull. Chem. Soc. Jpn.*, 1974, **47**, 767.
- 23 J. M. Cole, K. F. Bowes, I. P. Clark, K. S. Low, A. Zeidler, A. W. Parker, I. R. Laskar and T. M. Chen, *Cryst. Growth Des.*, 2013, **13**, 1826.
- 24 H. J. Bae, J. Chung, H. Kim, J. Park, K. M. Lee, T. W. Koh, Y. S. Lee, S. Yoo, Y. Do and M. H. Lee, *Inorg. Chem.*, 2014, **53**, 128.
- 25 S. Lamansky, P. Djurovich, D. Murphy, F. Abdel-Razzaq, R. Kwong, I. Tsyba, M. Bortz, B. Mmui, R. Bau and M. E. Thompson, *Inorg. Chem.*, 2001, **40**, 1704.
- 26 S. K. Leung, K. Y. Kwok, K. Y. Zhang and K. K. W. Lo, *Inorg. Chem.*, 2010, **49**, 4984.
- 27 T. Hofbeck and H. Yersin, *Inorg. Chem.*, 2010, **49**, 9290.
- 28 Q. L. Xu, C. C. Wang, T. Y. Li, M. Y. Teng, S. Zhang, Y. M. Jing, X. Yang, W. N. Li, C. Lin, Y. X. Zhen, J. L. Zuo and X. Z. You, *Inorg. Chem.*, 2013, **52**, 4916.
- 29 M. Tavasli, T. N. Moore, Y. H. Zheng, M. R. Bryce, M. A. Fox, G. C. Griffiths, V. Jankus, H. A. Al-Attar and A. P. Monkman, *J. Mater. Chem.*, 2012, **22**, 6419.
- 30 S. Okada, K. Okinaka, H. Iwawaki, M. Furugori, M. Hashimoto, T. Mukaide, J. Kamatani, S. Igawa, A. Tsuboyama, T. Takiguchi and K. Ueno, *Dalton Trans.*, 2005, 1583.
- 31 A. B. Tamayo, B. D. Alleyne, P. I. Djurovich, S. Lamansky, I. Tsyba, N. N. Ho, R. Bau and M. E. Thompson, *J. Am. Chem. Soc.*, 2003, **125**, 7377.
- 32 J. Dai, K. F. Zhou, M. Li, H. Q. Sun, Y. Q. Chen, S. J. Su, X. M. Pu, Y. Huang and Z. Y. Lu, *Dalton Trans.*, 2013, **42**, 10559.
- 33 G. N. Li, Y. Zou, Y. D. Yang, J. Liang, F. Cui, T. Zheng, H. Xie and Z. G. Niu, *J. Fluoresc.*, 2014, **24**, 1545.
- 34 C. L. Ho, W. Y. Wong, Q. Wang, D. Ma, L. Wang and Z. Lin, *Adv. Funct. Mater.*, 2008, **18**, 928.
- 35 Y. Wang, N. Herron, V. V. Grushin, D. LeCloux and V. Petrov, *Appl. Phys. Lett.*, 2001, **79**, 449.
- 36 K. P. S. Zanoni, B. K. Kariyazaki, A. Ito, M. K. Brennaman, T. J. Meyer and N. Y. M. Iha, *Inorg. Chem.*, 2014, **53**, 4089.
- 37 S. Bettington, M. Tavasli, M. R. Bryce, A. Beeby, H. Al-Attar and A. P. Monkman, *Chem. – Eur. J.*, 2007, **13**, 1423.
- 38 M. K. Nazeeruddin, R. T. Wehgh, Z. Zhou, C. Klein, Q. Wang, F. D. Angelis, S. Fantacci and M. Grätzel, *Inorg. Chem.*, 2006, **45**, 9245.
- 39 W. Lee, T. H. Kwon, J. Kwon, J. Y. Kim, C. Lee and J. I. Hong, *New J. Chem.*, 2011, **35**, 2557.
- 40 A. Juris, V. Balzani, F. Barigelletti, S. Campagna, P. Belser and A. Vonzelewsky, *Coord. Chem. Rev.*, 1988, **84**, 85.
- 41 M. Frank, M. Nieger, F. Vögtle, P. Belser, A. Vonzelewsky, L. D. Cola, V. Balzani, F. Barigelletti and L. Flamigni, *Inorg. Chim. Acta*, 1996, **242**, 281.
- 42 K. A. King, P. J. Spellane and R. J. Watts, *J. Am. Chem. Soc.*, 1985, **107**, 1431.
- 43 CrysAlisPro Version 1.171.36.21, Agilent Technologies Inc., Santa Clara, CA, USA, 2012.
- 44 L. Palatinus and G. Chapuis, *J. Appl. Crystallogr.*, 2007, **40**, 786.
- 45 G. M. Sheldrick, *Acta Crystallogr., Sect. A: Found. Crystallogr.*, 2008, **64**, 112.
- 46 O. V. Dolomanov, L. J. Bourhis, R. J. Gildea, J. K. Howard and H. Puschmann, *J. Appl. Crystallogr.*, 2009, **42**, 339.
- 47 M. J. Frisch, G. W. Trucks, H. B. Schlegel, G. E. Scuseria, M. A. Robb, J. R. Cheeseman, J. A. Montgomery, T. Vreven, K. N. Kudin, J. C. Burant, J. M. Millam, S. S. Iyengar, J. Tomasi, V. Barone, B. Mennucci, M. Cossi, G. Scalmani, N. Rega, G. A. Petersson, H. Nakatsuji, M. Hada, M. Ehara, K. Toyota, R. Fukuda, J. Hasegawa, M. Ishida, T. Nakajima, Y. Honda, O. Kitao, H. Nakai, M. Klene, X. Li, J. E. Knox, H. P. Hratchian, J. B. Cross, C. Adamo, J. Jaramillo, R. Gomperts, R. E. Stratmann, O. Yazyev, A. J. Austin, R. Cammi, C. Pomelli, J. W. Ochterski, P. Y. Ayala,

- K. Morokuma, G. A. Voth, P. Salvador, J. J. Dannenberg, V. G. Zakrzewski, S. Dapprich, A. D. Daniels, M. C. Strain, O. Farkas, D. K. Malick, A. D. Rabuck, K. Raghavachari, J. B. Foresman, J. V. Ortiz, Q. Cui, A. G. Baboul, S. Clifford, J. Cioslowski, B. B. Stefanov, G. Liu, A. Liashenko, P. Piskorz, I. Komaromi, R. L. Martin, D. J. Fox, T. Keith, M. A. Al-Laham, C. Y. Peng, A. Nanayakkara, M. Challacombe, P. M. W. Gill, B. Johnson, W. Chen, M. W. Wong, C. Gonzalez and J. A. Pople, *Gaussian 09, Revision A.01*, Gaussian, Inc., Wallingford, CT.
- 48 C. Lee, W. Yang and R. G. Parr, *Phys. Rev. B: Condens. Matter Mater. Phys.*, 1988, **37**, 785.
- 49 B. Miehlich, A. Savin, H. Stoll and H. Preuss, *Chem. Phys. Lett.*, 1989, **157**, 200.
- 50 A. D. Becke, *J. Chem. Phys.*, 1993, **98**, 5648.
- 51 M. Cossi, N. Rega, G. Scalmani and V. Barone, *J. Comput. Chem.*, 2003, **24**, 669.
- 52 J. Tomasi, B. Mennucci and R. Cammi, *Chem. Rev.*, 2005, **105**, 2999.